Chiral Bis(amino alcohol)oxalamide Gelators—Gelation Properties and Supramolecular Organization: Racemate versus Pure Enantiomer Gelation

Janja Makarević,[a] Milan Jokić,[a] Zlata Raza,[b] Zoran Štefanić,[c] Biserka Kojić-Prodić,*[c] and Mladen Žinić*[a]

Abstract: Four new chiral bis(amino alcohol)oxalamides (**1**–**4**: amino alcohol = leucinol, valinol, phenylglycinol, and phenylalaninol, respectively) have been prepared as low-molecular-weight organic gelators. Their gelation properties towards various organic solvents and mixtures were determined and these were then compared to related bis(amino acid) oxalamide gelators. Spectroscopic (FTIR, ^{1}H NMR) and X-ray diffraction studies revealed that the primary organization motif of (*S*,*S*)-**1** and racemate **1** (*rac*-**1**) in lipophilic solvents involved the formation of inverse bilayers. The X-ray crystal structure of (*S*,*S*)-**1** also shows this type of bilayer organization. The crystal structure of *rac*-**2** reveals *meso* bilayers of hydrogen-bonded aggregates. Within the bilayers formed, the gelator molecules are connected by cooperative hydrogen bonding between oxalamide units and OH groups, while the interbilayer interactions are realized through lipophilic interactions between the *i*Bu groups of leucinol. Oxalamide *meso*-**1** lacks any gelation ability and crystallizes in monolayers. In dichloromethane r*ac*-**1** forms an unstable gel; this is prone to crystallization as a result of the formation of symmetrical *meso* bilayers. In contrast, in aromatic solvents r*ac*-**1** forms stable gels; this indicates that enantiomeric bilayers are formed. Oxalamide *rac*-**1** is capable of gelling a volume of toluene three times larger than (*S*,*S*)-**1**. A tranmission electron microscopy investigation of r*ac*-**1** and (*S*,*S*)-**1** toluene gels reveals the presence of thinner fibers in the former gel, and, hence, a more compact network that is capable of immobilizing a larger volume of the solvent. The self-assembly of these types of gelator molecules into bilayers and subsequent formation of fibrous aggregates can be explained by considering the strength and direction of aggregate forces (supramolecular vectors) in three-dimensional space.

Keywords: bilayers · gels · racemates · self-assembly · supramolecular chemistry

Introduction

The gelation phenomenon exhibited by low-molecular-weight organic compounds has recently attracted considerable attention.[1] Gels represent new soft materials that have numerous potential applications, for example, in slow drug delivery systems,[2] in sensing devices that respond to internal or external stimuli (pH, temperature, light, solute),[3] and as hardeners of liquid-waste materials.[4] It might also be envisaged that they can be used for the safer transport of dangerous liquids and as compartmental reaction or crystallization vessels. The supramolecular nature of the gelation phenomenon has been recognized. Gel fibers, usually of micrometer scale lengths and nanometer scale diameters, are formed in solution predominantly by the unidirectional self-assembly of gelator molecules.[5] The entanglement of many such fibers then gives a network, which traps the solvent in the network compartments. A number of highly efficient gelators capable of affecting gelation even at concentrations below 0.05 wt% have been prepared recently. However, the exact relationship between the gelator structure (constitution, configuration, and conformation), the properties of a solvent that can be gelled, and the motif of supramolecular organization within the gel fibers still remains to be established. Even very slight variations of gelator constitution and changes of conformation or configuration can tremendously influence

[a] Prof. M. Žinić, Dr. J. Makarević, Dr. M. Jokić
Laboratory of Supramolecular and Nucleoside Chemistry
Rudjer Bošković Institute
P.O. Box 180, 10002 Zagreb (Croatia)
Fax: (+385) 1-46-80-195
E-mail: zinic@rudjer.irb.hr

[b] Dr. Z. Raza
Laboratory for Stereoselective Catalysis and Biocatalysis
Rudjer Bošković Institute
P.O. Box 180, 10002 Zagreb (Croatia)

[c] Dr. B. Kojić-Prodić, Z. Štefanić
Laboratory for Chemical and Biological Crystallography
Rudjer Bošković Institute
P.O. Box 180, 10002 Zagreb (Croatia)
Fax: (+385) 1-46-80-245
E-mail: kojic@rudjer.irb.hr

Supporting information for this article is available on the WWW under http://www.chemeurj.org or from the author.

 DOI: 10.1002/chem.200304573

the gelation properties.[6] Gelator stereochemistry has a pronounced influence on the gelation properties. For chiral gelators, both enantiomers have equal gelation properties toward achiral solvents but symmetrical *meso* diastereoisomers lack any gelation.[7] It was also observed that, in most cases, racemates are less efficient gelators than pure enatiomers, and sometimes lack any gelation ability because of a strong tendency to crystallize.[8] The "chiral bilayer effect" was formulated to explain why pure enatiomers prefer to gel, while racemates of amphiphilic gelators prefer to crystallize.[9] However, the general validity of the effect is questionable.[10]

We have found that chiral bis(amino acid)oxalamides represent a group of versatile gelators that are able to gel water, as well as a number of low-polarity organic solvents. Spectroscopic studies combined with X-ray crystallography and molecular modeling have shed light on the relationship between their structural characteristics (configuration, conformation), gelation properties, and organization in gel fibers.[11] In the search for a new group of structurally related chiral gelators, the bis(amino alcohol) oxalamides **1**–**4** were prepared. Molecular modeling indicates that the minor

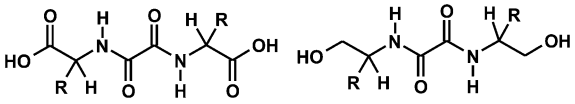

bis(amino acid) oxalamide gelators

bis(LeuOH)
bis(ValOH)
bis(PhGlyOH)
bis(PheOH)

bis(amino alcohol)oxalamide gelators

(*S*,*S*)-**1**
meso-**1** **R** = *i*Bu
rac-**1**

(*S*,*S*)-**2** **R** = *i*Pr
rac-**2**

(*R*,*R*)-**3** **R** = Ph
(*S*,*S*)-**4** **R** = CH_2Ph

constitutional differences between **1**–**4** and bis(amino acid)-oxalamide gelators in general (that is, the presence of hydroxymethylene instead of carboxylic groups) does not change their low-energy conformations. Since hydroxyl groups can also participate in intermolecular hydrogen bonding, as can the carboxylic groups of amino acid gelators, it was considered that the gelation properties of **1**–**4** could be predicted. Here, we present the results of the gelation studies of **1**–**4**, and show that the relatively small constitutional differences between bis(amino alcohol)- and bis(amino acid)-oxalamide gelators results in a dramatic change of the gelation properties. We also report on the first racemate (*rac*-**1**) to exhibit better gelling properties in toluene than the pure enatiomer [(*S*,*S*)-**1**].

Results and Discussion

Gelation experiments: The results of gelation experiment with **1**–**4** in various solvents and solvent mixtures are given in Table 1. Gelation efficiency is expressed by the maximal volume (V_{max}) of the solvent or solvent mixture upon being gelled by 10 mg of a gelator. Comparison of the gelation properties of (*S*,*S*)-**1** and bis(LeuOH)oxalamide reveals striking differences. The LeuOH derivative is able to gel highly-polar solvents and their mixtures, such as water, water/DMSO, and water/DMF,[11] whereas (*S*,*S*)-**1** is unable to gel any of these systems. Compounds (*S*,*S*)-**2** and **3** were observed to weakly gel a water/DMSO mixture (water/DMSO, 1.3:1; $V_{max} = 0.8$ mL, Table 1). Although soluble in pure dioxane and THF, (*S*,*S*)-**1** efficiently gelled 1:7 (v/v) mixtures of dioxane/THF with hexane; minimal gelation concentrations of 0.05 and 0.04 wt% ($g ml^{-1}$), respectively, constitute a "supergelator".[12] However, *rac*-**1** showed much less efficient gelation of the same solvent mixtures, and gave unstable gels that were prone to crystallization. Apolar CCl_4 and aromatic solvents can be efficiently gelled by (*S*,*S*)-**1**. *Rac*-**1** also gave stable gels with these solvents but gelation was less efficient, except in the case of toluene (Table 1). The valinol and phenylglycinol derivatives **2** and **3**, respectively, do not gel any of the aromatic solvents, whereas the phenylalaninol derivative **4** showed moderate gelation. Relative to (*S*,*S*)-**1**, the bis(LeOH) derivative was up to 20 times less efficient in gelling benzene, and was also much less efficient in gelling other aromatic solvents (V_{max} for benzene, toluene, *o*-, *m*-, and *p*-xylene 0.5, 1.8, 1.15, 1.1, 1.20 mL, respectively), while the bis(PhGlyOH) and bis(PheOH) derivatives did not gel any of these solvents. The bis(ValOH) derivative did not gel benzene and toluene, but showed very good gelation of *o*-, *m*-, and *p*-xylene (V_{max} 15.9, 21.0, and 17.8 mL, respectively).

Table 1. Gelation of various solvents and solvent mixtures by 10 mg of gelator.[a] Gelation efficiency expressed as the maximal volume of gelled solvent V_{max} [mL].

Solvent	(*S*,*S*)–**1**	*rac*–**1**	**3**	**4**
water	–[b]	–	–	–
water + DMSO	–	f[c]	1.1:1; 7	–
EtOH	–	–	4.65	1.4
dioxane	–	–	–	–
dioxane + hexane	1:7; 18.4	1:3.3; 2.1[d]	–	1:0.9; 2.1
THF	–	–	0.75	0.65
THF + hexane	1:7; 23.1	1:3; 3.2[d]	–	1.1:1; 5.4
EtOAc	–	–	–	2.0
EtOAc + hexane	1:1; 2.7	–	–	–
acetone	–	–	0.55	–
acetone – hexane	1.4:1; 0.6	–	–	–
CH_2Cl_2	4.1	0.9[d]	3.4	–
CH_2Cl_2 – hexane	1:1.4; 12.0	1:1.1; 7.0[d]	–	–
CCl_4	15.3	12.7	–	–
$CHCl_3$	2.0	0.9	–	–
benzene	9.9	7.9	–	–
toluene	5.0	15.0	–	8.0
o – xylene	13.9	8.6	–	8.2
m – xylene	9.5	1.5	–	6.0
p – xylene	8.5	2.0	–	6.0

[a] Detailed gelation testing procedure is described in ref. [11]; in most cases transparent gels were formed. [b] Denotes no gelation; solution or precipitate formed. [c] Denotes formation of solid fibers. [d] Unstable gels prone to crystallization.

The gelation experiments reveal the following: 1) (*S*,*S*)-**1** is a superior gelator relative to the valinol derivative (*S*,*S*)-**2** and the aromatic amino alcohol derivatives (*R*,*R*)-**3** and (*S*,*S*)-**4**; 2) the major difference between the amino acid and amino alcohol oxalamide gelators is that the former efficiently gel

highly polar solvent systems, while the latter do not gel them at all; 3) the common property of (*S*,*S*)-**1** and bis(LeuOH) derivatives is that they gel aromatic solvents; 4) for both types of gelators, the *meso*-bis(LeuOH) and *meso*-**1** diastereoisomers lacked any gelation; and 5) *rac*-**1** is capable of gelling the same solvent mixtures as (*S*,*S*)-**1**, but the gels formed are unstable and are prone to crystallization (*rac*-**1** gels other solvents less efficiently than (*S*,*S*)-**1** with the exception of toluene). Surprisingly, *rac*-**1** immobilizes a larger volume (×3) of toluene than (*S*,*S*)-**1**. To the best of our knowledge, *rac*-**1** represents the first example of a racemate that gels solvents better than the pure enantiomer. The following spectroscopic and crystallographic studies were undertaken to shed more light on the self-assembly motifs of (*S*,*S*)-**1** and *rac*-**1** in toluene gels.

Transmission electron microscopy (TEM) investigation: TEM was used to determine the fiber thickness in (*S*,*S*)-**1** and *rac*-**1** toluene gels. Figure 1 (top left), which shows the (*S*,*S*)-**1** gel network after staining with dipotassium phosphotungstate (PWK), has large fiber bundles (diameters in the 12–92 nm range). Although staining of the *rac*-**1** gel sample (Figure 1, top right) was less efficient, thinner fibers (diameters in the 4–24 nm range) relative to those of the (*S*,*S*)-**1** gel could be observed. Figure 1 (bottom panels), which were obtained by shading the gel samples with Pd, also show that the (*S*,*S*)-**1** gel network contains considerably thicker fibers than the *rac*-**1** gel.

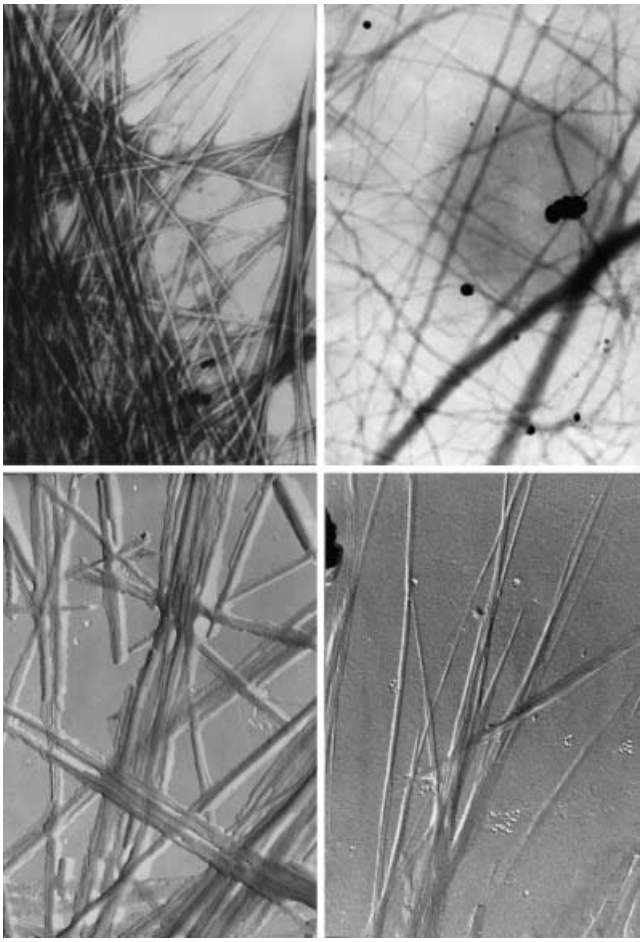

Figure 1. TEM images (25000×) of the (*S*,*S*)-**1** and *rac*-**1** toluene gels: (*S*,*S*)-**1** negatively stained with PWK (top left); *rac*-**1** without staining (top right); (*S*,*S*)-**1** shaded with Pd (bottom left); and *rac*-**1** shaded with Pd (bottom right).

FTIR investigations: To identify intermolecular interactions in toluene gel fibers in solution at 100 °C, as well as in the crystals of bis(leucinol) derivatives (*S*,*S*)-**1** and *rac*-**1**, the corresponding FTIR spectra were analyzed (Table 2). In the (*S*,*S*)-**1** and *rac*-**1** gel spectra at room temperature, the NH bands at 3294 and 3296 cm^{-1} and those of amide I at 1656 and 1654 cm^{-1} correspond to the hydrogen-bonded NH and CO functionalities of the oxalamide units, respectively. In the spectra of the solutions at 100 °C, both the NH and amide I bands shift to higher wave numbers (NH 3392 and 3387 cm^{-1}, and amide I 1681 and 1679 cm^{-1}); this indicates a disruption in the intermolecular hydrogen bonds between the oxalamide units of the gelator molecules. At the same time, the broad, low-intensity bands at 3600 cm^{-1} that appear in the solution spectra can be assigned to non-associated OH groups. These observations suggest that both the oxalamide and OH groups are involved in intermolecular hydrogen bonding which stabilizes the gel-fiber organization.

Table 2. Selected FTIR bands [$\tilde{\nu}$ in cm^{-1}] of (*S*,*S*)-**1** and *rac*-**1** toluene gels, solutions at 100 °C, and crystals.

	OH free	NH free	NH assoc.	amide I	amide II
(*S*,*S*)-**1** gel, RT	–	–	3294	1656	–[a]
(*S*,*S*)-**1** solution, 100 °C	3600	3392	–	1681	–[a]
(*S*,*S*)-**1** crystals	–		3378;[b] 3284	1654	1525
rac-**1** gel, RT	–	–	3296	1654	–
rac-**1** solution, 100 °C	3602	3387	–	1679	–
rac-**1** crystals	–		3365;[b] 3289	1654	1522

[a] Overlapped by toluene bands. [b] Denotes shoulder.

Neither NH nor amide I bands typical of non-hydrogen bonded species are observed in the spectra of gels at room temperature.[11] However, these bands (NH 3392, 3398 cm^{-1}; amide I 1681, 1654 cm^{-1} for (*S*,*S*)-**1** and *rac*-**1**, respectively) can be detected in the spectra recorded at elevated temperatures (Figure 1 in the Supporting Information). These observations strongly suggest that most of the gelator molecules are aggregated at room temperature. In the FTIR spectra of (*S*,*S*)-**1** and *rac*-**1** crystals, which were grown from ethanol/pentane and dichloromethane, respectively, the different shoulder positions at 3378 (for (*S*,*S*)-**1**) and 3365 cm^{-1} (for *rac*-**1**), as well as at the NH (3284 and 3289 cm^{-1}) and amide II bands (1525 and 1522 cm^{-1}), might indicate that the oxalamide units are subject to different hydrogen-bonding systems (see the paragraph on crystal structures).

^{1}H NMR investigations: The spectra for the (*S*,*S*)-**1** and *rac*-**1** [D_8]toluene gels at room temperature show the residual non-deuterated toluene signals and only traces of gelator. When the temperature was increased, the gelator signals became stronger and reached maximal intensity at temperatures beyond the gel melting point (Figure 2 in the Supporting

Information). Thus, at room temperature the gelator molecules are self-assembled in a rigid network, but upon heating, the network disintegrates into smaller, dissolvable, and NMR spectroscopically observable aggregates.[13] The presence of aggregated gelator molecules in solution was detected upon addition of 20 μL of [D_6]DMSO to the (*S*,*S*)-**1** [D_8]toluene gel (0.8 mL). As a result of strong gelator–DMSO hydrogen bonding, the gel network was completely destroyed to give an isotropic solution. On the other hand, the addition of only 5 μL of [D_6]DMSO preserves the gel state but increases the gelator signals; an effect that is also observed upon heating the gel sample. In both cases, the concentration of NMR observable entities dissolved in entrapped toluene increased. In the one-dimensional nuclear Overhauser enhancement spectroscopy (NOESY) experiments for the solution that contains 20 μL of [D_8]DMSO, positive nuclear Overhauser effects (NOEs), which are compatible with the presence of monomeric, non-aggregated gelator molecules, were observed. However, negative NOEs were obtained for the gel sample that contained only 5 μL of [D_6]DMSO (Figure 3 in the SupportingInformation). Negative NOEs are known to appear in the spectra of macromolecules with a molecular weight in excess of 1500.[1b] Therefore, their occurrence in the gel spectrum clearly shows that aggregates of at least six gelator molecules are present in the entrapped toluene. To acquire further information on gel-fiber organization, temperature-dependent spectra of solutions of (*S*,*S*)-**1** and *rac*-**1** in [D_8]toluene were recorded and analyzed. Solutions that had concentrations just below the minimal gelation concentration of each gelator were viscous, because of the presence of highly aggregated gelator molecules. As a result, organization in such aggregates and gel fibers should be very similar. The temperature-dependent chemical shifts for all of the (*S*,*S*)-**1** protons, except OH, are shown in Figure 2. Similar shift tendencies were obtained for the *rac*-**1** protons (not shown). For the NH, C*H, and methylene protons of the CH_2OH groups, two chemical shift trends can be observed, namely downfield shifts in the 40–60 °C range, and upfield shifts in the 60–90 °C range. Disintegration of the oxalamide–oxalamide and OH···OH hydrogen bonding explains the upfield shifts for NH and the methylene protons of the CH_2OH groups at higher temperatures; this was also observed in the temperature-dependent FTIR spectra (Figure 1 in the Supporting Information). The C*H protons oriented parallel to the oxalamide carbonyl groups (see Figure 2) are also shifted upfield at higher temperatures, presumably, because of an increase in the electron density on the oxalamide carbonyl oxygen atoms upon the destruction of the hydrogen bonds.

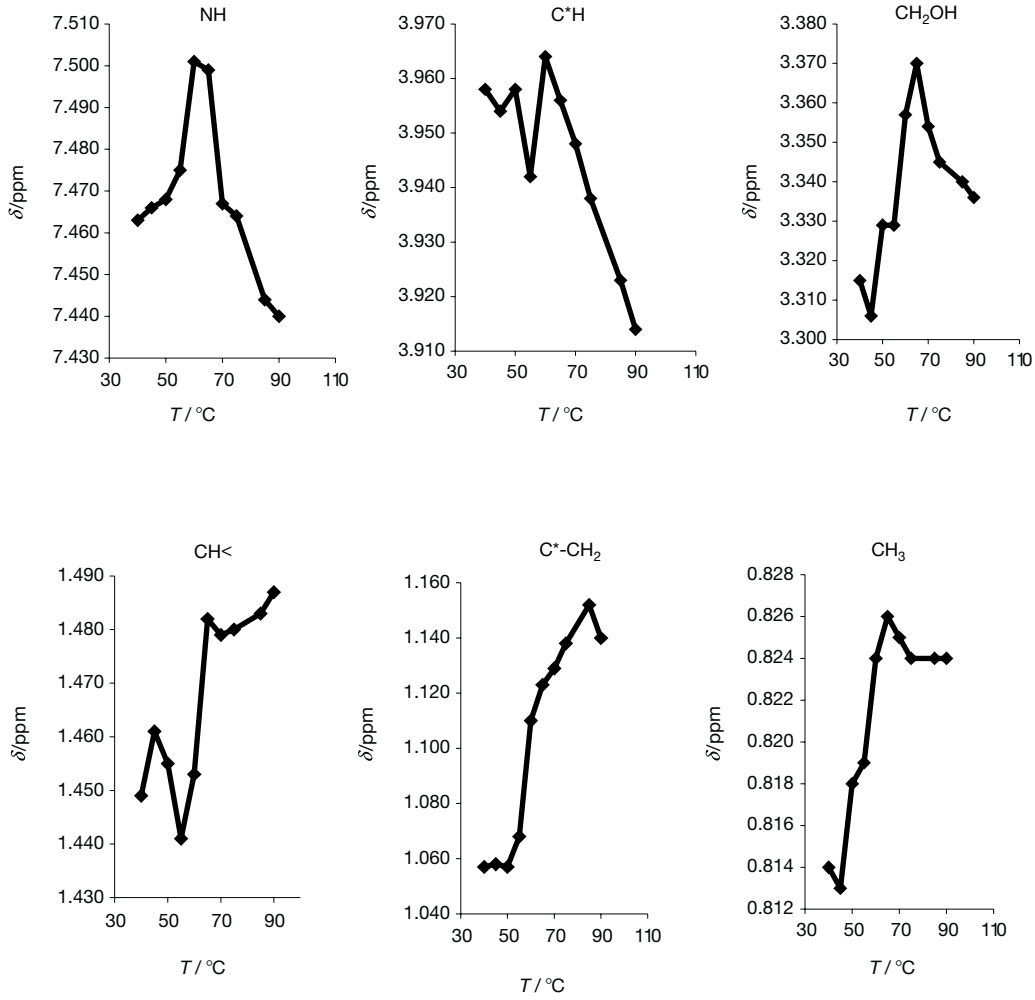

Figure 2. The chemical shifts of the (*S*,*S*)-**1** protons in a [D_8]toluene solution recorded between 40–90 °C.

The downfield shift of the NH, C*H, and methylene protons of the CH_2OH groups observed in the low-temperature range indicates that another type of energetically less-demanding disassembly is occurring to give smaller aggregates in which the protons are less shielded. The methylene (C^*-CH_2), methine (CH<), and methyl protons of the *i*Bu groups were shifted downfield when the temperature was increased. This suggests the presence of lipophilic interactions between the *i*Bu groups in the aggregates, whereby these protons are shielded but become deshielded upon disassembly. Thus, lipophilic interactions also stabilize the aggregates, and the observed deshielding effects in the low-temperature range suggest that the first and less energy-demanding disaggregation step occurs within the lipophilic regions of the aggregates. The NMR spectroscopy results for both (*S*,*S*)-**1** and *rac*-**1** suggest that the fiber organization is characterized by intermolecular hydrogen bonding of the oxalamides and OH groups, as well as by lipophilic interactions that involve *i*Bu groups. The same type of interaction is also found in the corresponding crystal structures (see next section).

To determine whether there was any significant difference in the thermal stability of (*S*,*S*)-**1** and *rac*-**1** toluene gels, which in turn would indicate different organization, ^{1}H NMR spectroscopy was used to monitor increases in dissolved gelator–aggregate concentrations as a function of increasing temperature (Figure 3, left). The concentration of dissolved aggregates (c_d) was calculated using the known concentration of the internal standard tetrachloroethane.[11] Since the experiments were performed in a temperature range below the gel melting point ($T < T_g$), the two equilibria shown in Equation (1) are in operation, as determined by Whitten.[13b]

$$G_n \rightleftharpoons G_{ma} \rightleftharpoons G_d \quad (1)$$

G_n denotes gelator molecules assembled in the rigid network, and, hence, are not observable by NMR spectroscopy. On the other hand, G_{ma} corresponds to larger mobile aggregates, while G_d are dissolved gelator molecules, both of which are observable by NMR spectroscopy, albeit they undergo fast exchange on the NMR timescale. The cumulative dissolution equilibrium constant can be defined as $K_d = [c_d]$ in which $[c_d] = [c_{G_{ma}}] + [c_{G_d}]$. The K_d values at different temperatures can be calculated,[11] and by plotting $\ln K_d$ against $1/T$, the cumulative dissolution enthalpy (ΔH_d) and entropy (ΔS_d) changes can be calculated according to the equation $\ln K_d = (-\Delta H_d/R)\,1/T + \Delta S_d/R$. For both gels, a linear $\ln K_d$ versus $1/T$ dependence was obtained (Figure 3, right; $R^2 > 0.99$); this indicates that each gel network disintegrates into aggregates of similar size. For (*S*,*S*)-**1** and *rac*-**1**, the ΔH_d values obtained were 93 ± 3 and 78 ± 0.5 kJ mol^{-1}, respectively, while the ΔS_d values were determined as 240 and 197 J K^{-1} mol^{-1}, respectively. At 25 °C, the following values were determined for the dissolution of the (*S*,*S*)-**1** gel: $\Delta G_d = 22$ kJ mol^{-1}, $\Delta H_d = 93$ kJ mol^{-1}, and $T\Delta S_d = 71$ kJ K^{-1} mol^{-1}. On the other hand, the dissolution of the *rac*-**1** gel gave $\Delta G_d = 19$ kJ mol^{-1}, $\Delta H_d = 78$ kJ mol^{-1}, and $T\Delta S_d = 59$ kJ K^{-1} mol^{-1}. It appears that both dissolution processes are slightly enthalpy controlled. The curves in Figure 3 show that the *rac*-**1** gel network dissolves only slightly faster than (*S*,*S*)-**1**, and, therefore, lower thermodynamic parameters were obtained. These results seem to contradict the lower minimal gelation concentration (mgc) of *rac*-**1**, and imply that it has a lower solubility in toluene. However, the TEM images of the (*S*,*S*)-**1** and *rac*-**1** gels show the presence of thin fiber bundles for the latter gel. Consequently, *rac*-**1** cleaves to give mobile aggregates (G_{ma}) observable by NMR spectroscopy at lower temperatures relative to the (*S*,*S*)-**1** gel. In other words, G_{ma} contributes to a larger extent to the cumulative increase of c_d for the *rac*-**1** gel than for the (*S*,*S*)-**1** gel. Hence, in the $T < T_g$ temperature regime, the difference in solubility and thermodynamic parameters reflects the difference in the gel network fiber dimensions.

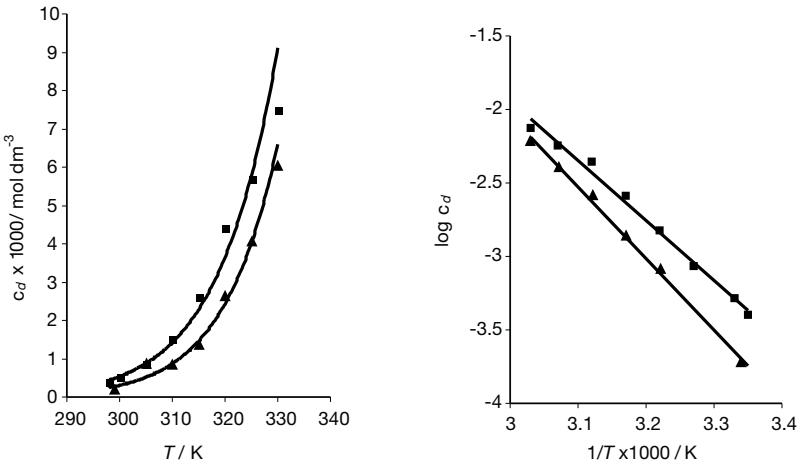

Figure 3. Increases in the concentration of dissolved, ^{1}H NMR observable aggregates (c_d) as a function of temperature for (*S*,*S*)-**1** (▲) and *rac*-**1** (■) toluene gels (left), and the linear dependence of log c_d versus $1/T$ for (*S*,*S*)-**1** (▲) and *rac*-**1** (■) toluene gels (right).

Molecular structures of (*S*,*S*)-1, *rac*-1, *meso*-1, and *rac*-2: Molecular conformations (Figure 4) are described by selected torsional angles (Tables 3 and 4), and are labeled in accordance with IUPAC–IUBMB nomenclature.[14] For the structure determination of **1**, the *S*,*S* enantiomer was selected based on the precursor configuration used in the synthesis. The ORTEP-III[15] drawing of *rac*-**1** (Figure 4) reveals an asymmetric unit that contains $1 + \frac{1}{2}$ molecules. A crystallographic twofold axis perpendicular to the C–C oxalamide bond generates the second half of the molecule in which the *cis*-oriented leucyl residues are located as in the (*S*,*S*)-**1** molecule. The centrosymmetric space group *C*2/*c* includes symmetry operations that invert the absolute configuration of the molecule to give the racemate. Compound *meso*-**1** has C_i molecular symmetry. The two crystallographically independent halves

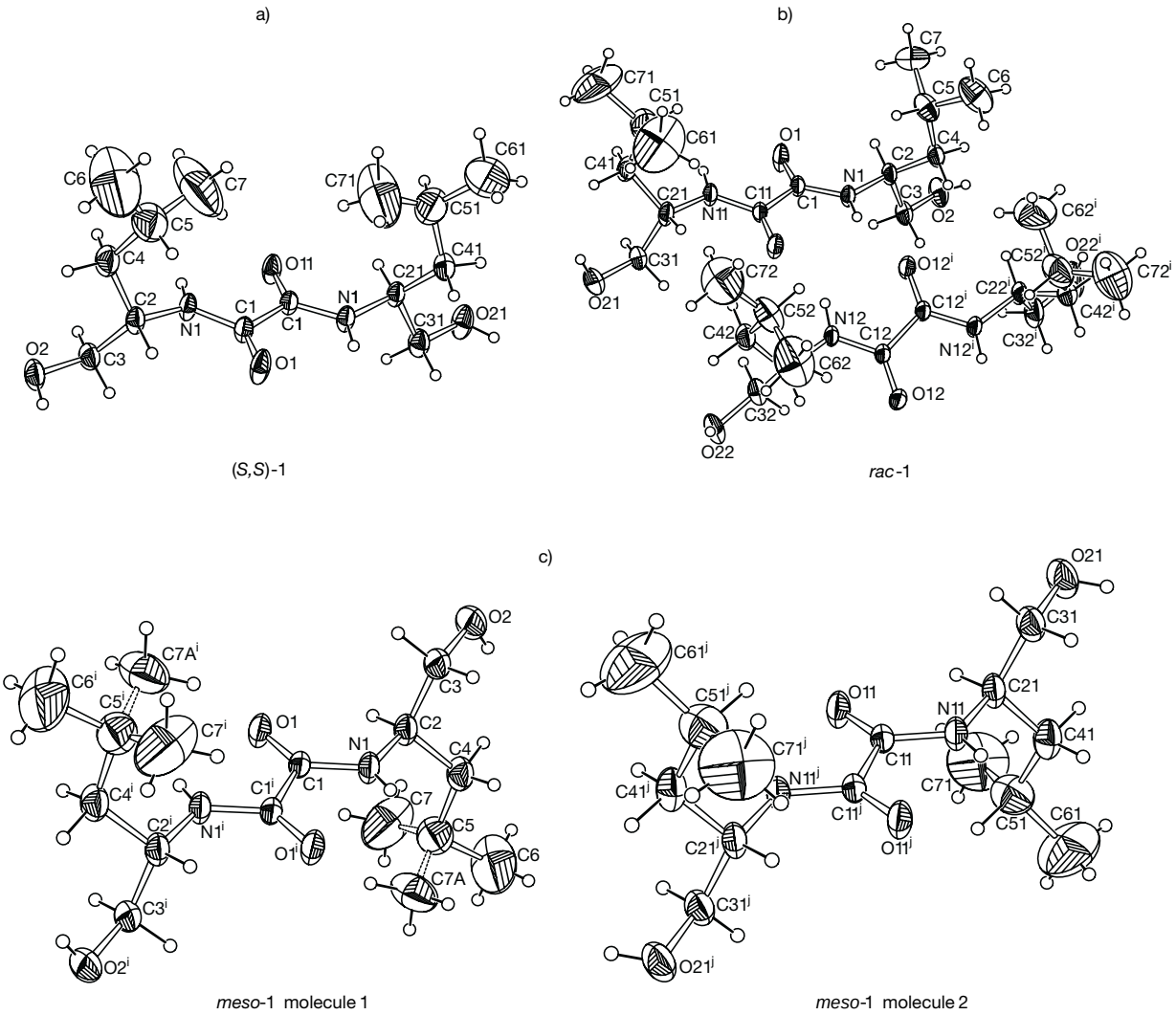

Figure 4. Molecular structures of: a) (*S*,*S*)-**1** with 30% probability displacement ellipsoids; b) *rac*-**1** with 30% probability displacement ellipsoids in which the asymmetric unit consists of 1+½ molecules, and the superscript *i* defines the symmetry operation -*x*, *y*, ½ – *z*; and c) two asymmetric units of *meso*-**1** with 30% probability displacement elipsoids and symmetry operations marked by superscripts $i = -x, 2-y, 2-z$, and $j = -x, 1-y, -z$.

Table 3. Selected torsional angles of (*S*,*S*)-**1** and *rac*-**1** [°].

		(*S*,*S*)-**1**	*rac*-**1**		*rac*-**1**[a]
ω	C2-N1-C1-C11	– 174.0(3)	– 178.2(3)		
ω'	C21-N11-C11-C1	– 172.8(3)	– 179.6(3)	C22-N12-C12-C12^{i}	180.0(4)
ϕ	C1-N1-C2-C3	– 114.2(4)	– 97.4(4)		
ϕ'	C11-N11-C21-C31	– 110.7(4)	– 95.8(4)	C12-N12-C22-C32	– 99.3(4)
χ	N1-C2-C4-C5	– 66.7(5)	– 68.0(4)		
χ'	N11-C21-C41-C51	– 74.7(5)	– 69.9 (5)	N12-C22-C42-C52	– 62.2(4)
ψ	N1-C2-C3-O2	178.7(3)	174.0(3)		
ψ'	N11-C21-C31-O21	175.1(3)	179.3(3)	N12-C22-C32-O22	175.3(4)

Table 4. Selected torsional angles of *meso*-**1** [°].[a]

	Molecule 1		Molecule 2	
ω	C2-N1-C1-C1^{i}	– 179.4(3)	C21-N11-C11-C11^{j}	– 178.9(3)
ϕ	C1-N1-C2-C3	98.4(4)	C11-N11-C21-C31	110.1(4)
χ	N1-C2-C4-C5	63.1(5)	N11-C21-C41-C51	70.6(5)
ψ	N1-C2-C3-O2	– 177.9(3)	N11-C21-C31-O21	– 175.6(3)

[a] Symmetry operarions: $i = -x, 2-y, 2-z$; $j = -x, 1-y, -z$.

of the molecule are positioned around two centers of symmetry (at the special positions (0,0,0) and (0,½,0) of the space group $P\bar{1}$), which occur in the middle of the oxalamide bridges. Therefore, the leucyl residues are situated on opposite sides of the oxalyl bridge. All these molecules are characterized by the two oxygen atoms of the *trans*-disposed oxalamide units (ORTEP-III drawings, Figure 4). The terminal isopropyl groups of the molecules studied had high thermal parameters. In one *meso*-**1** conformer, the terminal methyl group is split into two equally populated locations (atoms C7 and C7A, Figure 4c).

Hydrogen bonding and crystal packing of (*S*,*S*)-1, *rac*-1, *meso*-1, and *rac*-2: The crystal packing of (*S*,*S*)-**1** is characterized by a two-dimensional hydrogen-bonded pattern in the *ab* plane (Figure 5). Intra- and intermolecular hydrogen bonds between the oxalamide groups creates a "ladder" pattern that runs along the *b* plane (Figure 5, Table 5). The chain formed contains intramolecular hydrogen bonds (N1–H1 ··· O11 and N11–H11 ··· O1), which generate five-membered rings

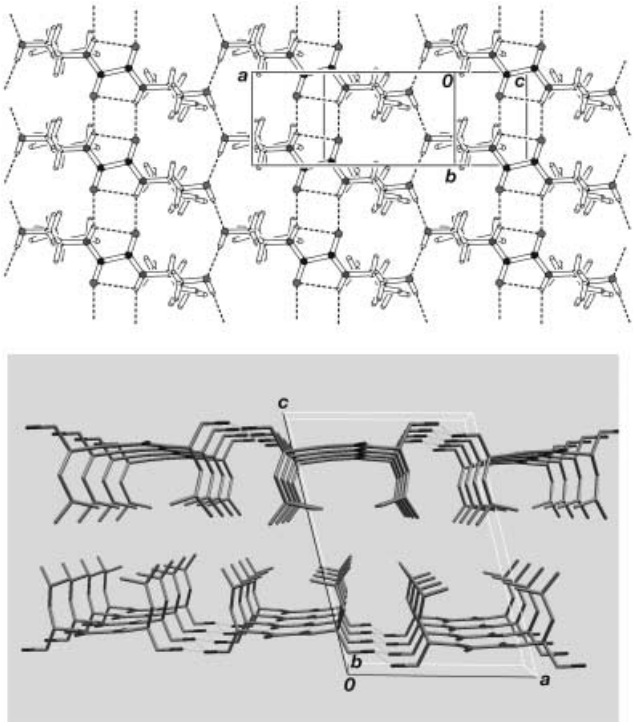

Figure 5. Top: the hydrogen bonding network in the crystal structure of (*S*,*S*)-**1** in the *ab* plane. Bottom: the hydrophobic channel between leucyl groups in the (*S*,*S*)-**1** crystal structure.

Table 5. Hydrogen-bond geometry in the crystal structure of (*S*,*S*)-**1**.

	D–H [Å]	H···A [Å]	D···A [Å]	D–···A [°]	Graph set descriptor
O2–H2O···O21[a]	0.82	1.994	2.814(5)	177	**C(11)**
O21–H21O···O2[b]	0.82	1.968	2.757(5)	161	**C(11)**
N1–H1···O1[c]	0.86	2.089	2.888(4)	154	**C(4)**
N1–H1···O11	0.86	2.305	2.691(3)	107	**S(5)**
N11–H11···O1	0.86	2.326	2.706(3)	107	**S(5)**
N11–H11···O11[d]	0.86	2.093	2.897(3)	155	**C(4)**

[a] $1+x, y, z$. [b] $-1+x, 1+y, z$. [c] $x, -1+y, z$. [d] $x, 1+y, z$.

(pseudo-C_5 pattern related to a peptide C_5) that are described by the descriptor **S(5)**.[16] The intermolecular hydrogen bonds (N1–H1···O1 and N11–H11···O11) complete the infinite motif along *b*; this is described by the unitary graph-set descriptor **C(4)**. The chain also includes patterns defined by the graph-set descriptors $\mathbf{R_2^2(4)}$ and $\mathbf{R_2^2(10)}$. Laterally located OH groups participate in hydrogen bonds (O1–H20···O21 and O21–H21O···O2; Figure 5 top, Table 5) that connect the chains into a two-dimensional pattern, described by Fowler and Lauher[17] as the β-network. The complete β-pattern is described by the unitary graph-set $\mathbf{N_1}$ = **C(4)S(5)S(5)C(4)C(11)C(11)**. In the crystal of (*S*,*S*)-**1**, the leucyl residues form a pronounced bilayered structure, which is separated by a hydrophobic channel (Figure 5 bottom). The crystal structure of *rac*-**1** is characterized by a two-dimensional hydrogen-bonded pattern in the *ac* plane (Figure 6 top). A basic "ladder" motif, which runs in the [10$\bar{1}$] direction, contains both intra- and intermolecular N–H···O hydrogen bonds between oxalamide groups (Figure 6, Table 6). It also includes the characteristic pseudo-C_5 intermolecular hydrogen bond, which is defined by the **S(5)** graph-set descriptor. Within this chain are rings which are

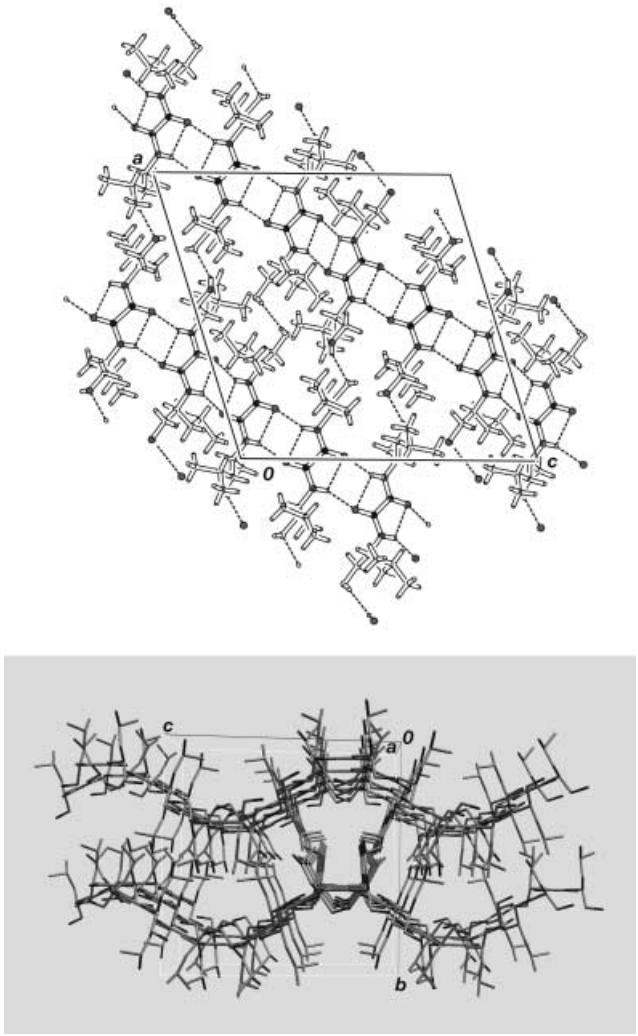

Figure 6. Top: the hydrogen bonding network of *rac*-**1** in the *ac* plane. Bottom: the arrangement of hydrophobic groups between the wave hydrogen-bonded planes.

Table 6. Hydrogen-bond geometry in the crystal structure of *rac*-**1**.

	D–H [Å]	H···A [Å]	D···A [Å]	D–H···A [°]	Graph set descriptor
O2–H2O···O22[a]	0.82	2.140	2.786	135	$\mathbf{D_2^2(12)}$
O21–H21O···O21[b]	0.82	2.411	2.865	115	$\mathbf{R_2^2(4)}$
O22–H22O···O2[c]	0.82	2.279	2.786	120	**S(5)**
N11–H11N···O1	0.86	2.328	2.701	106	$\mathbf{R_2^2(10)}$
N11–H11N···O1[d]	0.86	2.124	2.888	147	$\mathbf{D_2^2(6)}$
N1–H1N···O12[e]	0.86	2.126	2.943	158	**S(5)**
N1–H1N···O11	0.86	2.362	2.724	105	$\mathbf{D_2^2(8)}$
N12–H12N···O11	0.86	2.097	2.880	151	**S(5)**

[a] $-0.5+x, 0.5-y, -0.5+z$. [b] $1-x, y, 0.5-z$. [c] $0.5+x, 0.5-y, 0.5+z$. [d] $0.5-x, 0.5-y, -z$. [e] $-x, y, 0.5-z$.

defined by the binary graph-set descriptors $\mathbf{R_2^2(4)}$ and $\mathbf{R_2^2(10)}$. Owing to the space group symmetry operations applied to the $1+½$ crystallographically independent molecules, this "ladder" pattern is composed of molecular triads of opposite chirality: molecules that are operated by a twofold rotation or translation keep the same chirality, whereas those that are operated by inversion or glide plane change chirality (Figure 6 top). Thus, the generated sequence is *SS*,*SS*,*SS*,*RR*,*RR*,*RR*. Hydrogen bonds between the terminal hydroxyl groups (O−H···O) connect the "ladder"-type chains to give the two-dimensional network (Figure 6, Table 6). These terminal hydroxyl groups form tandem hydrogen bonds: O2−H2O···O22 and O21−H21O···O2 connect molecules of opposite chirality, whereas O21−H21O···O21 joins molecules that are related by the twofold rotation symmetry and have the same chirality.

The crystal packing of *meso*-**1** is characterized by a two-dimensional hydrogen-bonded pattern in the *bc* plane. Intra- and intermolecular hydrogen bonds between oxalamide groups create a "ladder" pattern, which runs along the *b* axis (Figure 7, Table 7). The chain formed contains intramolecular hydrogen bonds (N1−H1···O1 and N11−H18···O11), which generate five-membered rings (pseudo-C_5) that are described by the descriptor **S(5)**.[16] The intermolecular hydrogen bonds N1−H1···O11 and N11−H18···O1 complete the infinite motif along the *b* axis. Hydrogen bonds O2−H5···O21 and O21−H22···O2 (Figure 7 top, Table 7) connect the chains in a two-dimensional pattern, described by Fowler and Lauher[17] as the β-network. The hydrogen atoms of the lateral hydroxyl groups seem to have somewhat disordered positions. They were located during refinement by having their torsional angles fixed at maximum density around the oxygen atoms. The complete β-pattern is described by the unitary graph-set $\mathbf{N_1 = DDDS(5)DS(5)}$. The leucyl residues are arranged on both sides of the plane of hydrogen bonds (Figure 7 bottom).

Table 7. Hydrogen-bond geometry in the crystal structure of *meso*-**1**.

	D−H [Å]	H···A [Å]	D···A [Å]	D−H···A [°]	Graph set descriptor
N1−H1···O1 [a]	0.74(4)	2.37(4)	2.703(3)	109(3)	**S(5)**
N1−H1···O11 [b]	0.74(4)	2.21(4)	2.897(3)	155(4)	**D**
O2−H5···O21 [c]	0.82	2.43	2.726(5)	103	**D**
N11−H18···O1[d]	0.82(4)	2.16(4)	2.910(4)	154(3)	**D**
N11−H18···O11[e]	0.82(4)	2.31(3)	2.702(4)	110(3)	**S(5)**
O21−H22···O2[f]	0.82	1.91	2.726(5)	170	**D**

[a] $-x, 2-y, 2-z$. [b] $-x, 2-y, 1-z$. [c] $x, 1+y, z$. [d] $-x, 1-y, 1-z$. [e] $x, 1+y, z$. [f] $x, -1+y, z$.

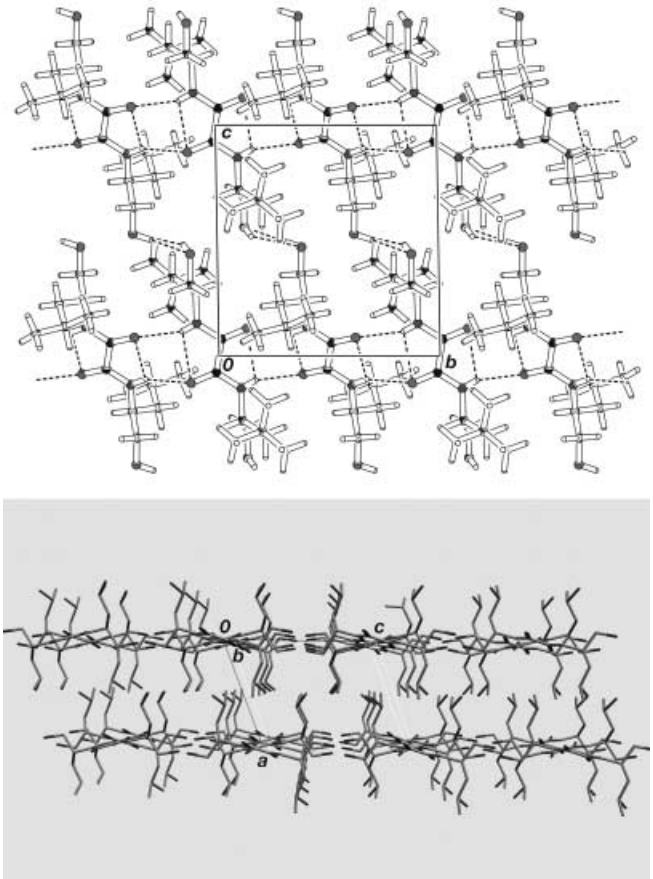

Figure 7. Top: the two-dimensional hydrogen-bonded β-network of *meso*-**1** in the *bc* plane. Bottom: the hydrophobic groups in the crystal structure of *meso*-**1** arranged between planes of hydrogen bonds in which a single orientation of the disordered methyl group is shown.

The crystal packing of *rac*-**2** reveals a pattern that is different to the one described in the crystal structures of **1**. The terminal alcohol groups that have a *syn* hydrogen atom , generated by an inversion symmetry, through the O21−H21O···O2 hydrogen bond (Table 8) connect two molecules of opposite chirality into a ring. The rings so formed are interconnected by hydrogen bonds (N1−H1N···O1 and N11−H11N···O11), which occur between oxalamide groups in the *a* plane. Furthermore, inter- and intramolecular hydrogen bonds between oxalamide groups create a common "ladder" pattern (this involves the three-centered hydrogen bonds) along the *a* plane (Figure 8 top). The ladder pattern is common to all the structures described in this work and also in other retropeptides.[18–21] The O2 hydroxy group also participates in a hydrogen bond (O2−H2O···O1) with an oxalamide group. The oxalamide oxygen O1 acts as a double acceptor of protons (from O2−H2O and N1−H1N). The pattern that is generated by these hydgrogen bonds cannot be classified as a β-network. The valyl groups, which are oriented on the same side of the

Table 8. Hydrogen-bond geometry in the crystal structure of *rac*-**2**.

	D−H [Å]	H···A [Å]	D···A [Å]	D−H···A [°]	Graph set descriptor
N1−H1N···O1 [a]	0.75(8)	2.25(8)	2.915(7)	150(7)	**C(4)**
N1−H1N···O11	0.75(8)	2.29(7)	2.682(7)	114(6)	**S(5)**
O2−H2O···O1 [a]	0.83(6)	1.98(6)	2.780(7)	162(5)	**C(7)**
N11−H11N···O1	0.71(6)	2.35(5)	2.706(7)	113(6)	**S(5)**
N11H11N···O11[b]	0.71(6)	2.25(7)	2.898(7)	152(6)	**C(4)**
O21−H21O···N11	0.78(8)	2.57(8)	2.877(8)	105(7)	**D**
O21−H21O···O2[c]	0.78(8)	2.19(8)	2.901(8)	152(9)	$\mathbf{R_2^2(22)}$

[a] $1+x, y, z$. [b] $-1+x, y, z$. [c] $2-x, -y, -z$.

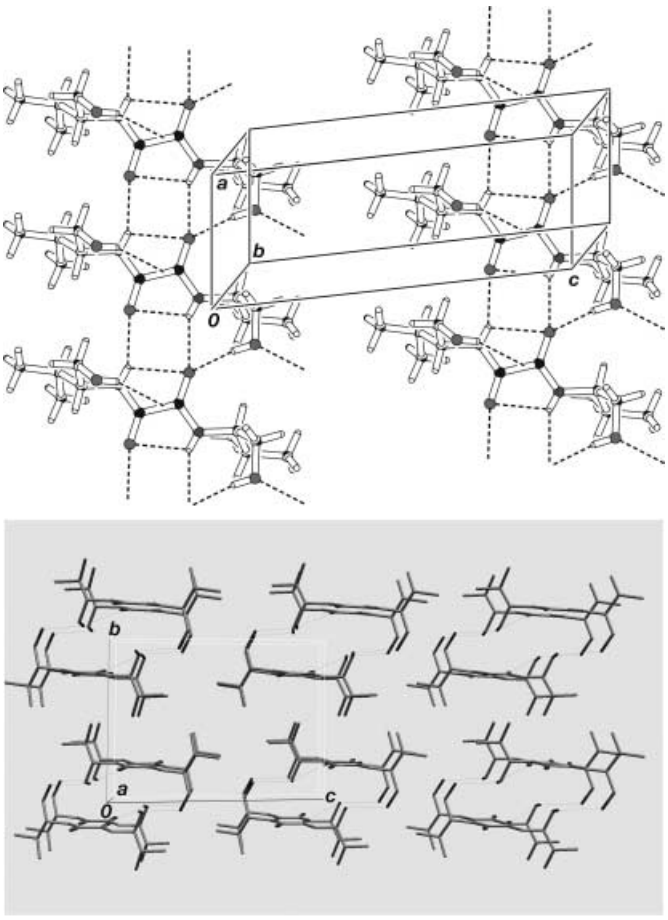

Figure 8. Top: the "ladder" motif along *a* in the structure of *rac*-**2**. Bottom: the layers of opposite chirality, which form the *meso* bilayers in the crystal structure of *rac*-**2**.

oxalamide backbone of two hydrogen-bonded aggregates of opposite chirality, form highly pronounced hydrophobic channels (Figure 8 bottom).

Organization of (*S*,*S*)-1 and *rac*-1 in toluene gels: Most of the chiral gelator racemates are either less efficient than their pure enatiomer counterparts, or do not have any gelation properties at all.[8] Fuhrhop's "chiral bilayer effect", which was formulated for amphiphilic gelators, predicts that enantiomers will form stable micellar fibers, while racemates will crystallize as *meso* bilayers.[9] The crystal structures of (*S*,*S*)-**1** and *rac*-**2** (Figures 5 and 8, respectively) clearly show a bilayer type of organization in the solid state. The molecular and molecular modelling structures of (*S*,*S*)-**1**, *rac*-**1**, and *rac*-**2** display rigid conformations that have clearly separated lipophilic and hydrophilic domains (Figure 4). Hence, these types of gelators may be considered as a special type of amphiphile, namely one which contains a hydrogen-bonded core. Both the crystal structures and the results of the ^{1}H NMR spectroscopy investigations strongly suggest that the gel fibers are organized into inverse bilayers. In light of these results, we propose an inverse bilayer model for the primary organization of both (*S*,*S*)-**1** and *rac*-**1** in the formation of gel fibers in toluene (Figure 9).

In this model, *rac*-**1** could form symmetric *meso* bilayers, which consist of *S* and *R* counterparts, and enantiomeric bilayers (Figure 9b and c, respectively). However, in contrast to *rac*-**2**, which possesses a *meso* bilayer type of crystal structure (Figure 7, from dichloromethane), the crystal structure of *rac*-**1** (Figure 6, from dichloromethane) displayed a waved organizational motif, which consisted of hydrogen-bonded triads of opposite chirality.

The ageing processes of (*S*,*S*)-**1** and *rac*-**1** toluene gels were examined by X-ray powder diffraction using an X'-PERT Philips 3040 powder diffractometer. A single, crystalline phase was observed when the spectra for both the (*S*,*S*)-**1** and *rac*-**1** gels were recorded while the solvent was evaporated. This was also observed for the xerogels prepared from toluene. As separation of the crystalline phases is fast (within 2–3 minutes), it would be reasonable to expect only a small structural rearrangement of the gel aggregates during the

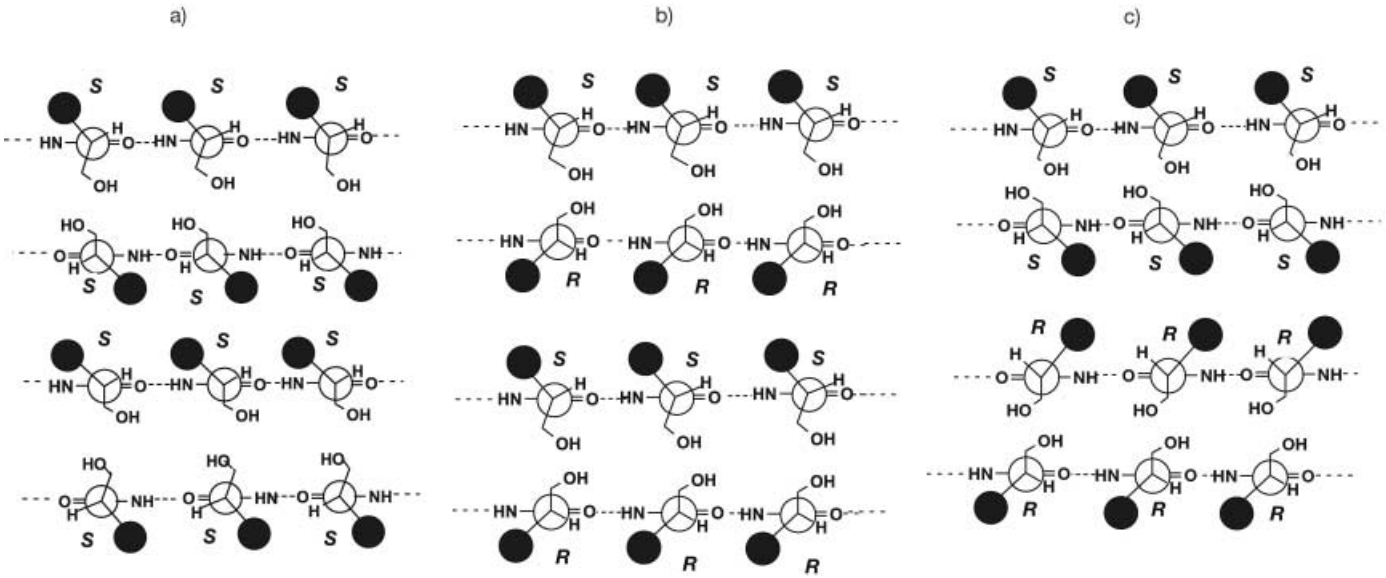

Figure 9. Proposed model for the inverse bilayer primary organization (partial Newman projection; *i*Bu groups are indicated by filled circles) of a) (*S*,*S*)-**1**; b) *meso* bilayer of *rac*-**1**; c) enatiomeric bilayers of *rac*-**1** in the toluene gel.

phase transition. A powder sample, which was prepared by grinding (*S*,*S*)-**1** single crystals, revealed a pattern analogous to the one recorded for the gel (Figure 10). Thus, the X-ray powder diffraction patterns of the crystalline phases of the

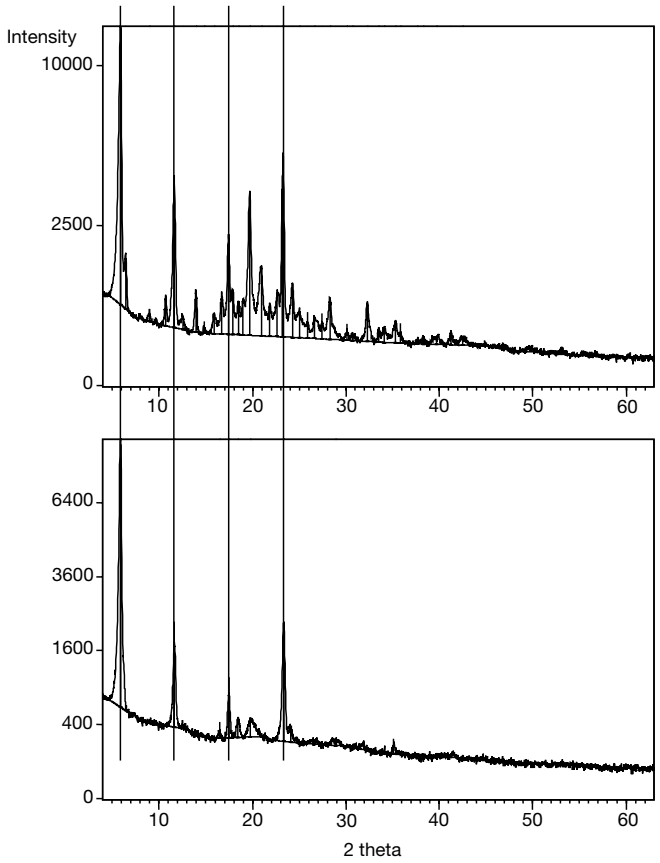

Figure 10. X-ray powder diffraction patterns of ground single crystals of (*S*,*S*)-**1** (upper panel); the tiny gel fibers of the *rac*-**1** toluene gel (lower panel) reveals the presence of the same lines, namely the most intensive ones, in both diagrams.

(*S*,*S*)-**1** and *rac*-**1** toluene gels, as well as the (*S*,*S*)-**1** single crystal suggest a close structural relationship for both gels, namely the formation of bilayers. In contrast, the crystalline phase of *rac*-**1**, which was obtained by crystallization from dichloromethane (see Figure 6), is different from that shown in Figure 10. A structural similarity with the phase detected in gels and xerogels is not observed. Since *rac*-**2** forms *meso* bilayers in dichloromethane, we assumed that the closely related *rac*-**1** may also form a *meso* bilayer. However, it appears that upon initial formation of a *meso* bilayer, *rac*-**1** undergoes subsequent reorganization as it slowly crystallizes from diluted dichloromethane. The FTIR data for (*S*,*S*)-**1** and *rac*-**1** dichloromethane gels (Figure 11) support this assumption.

While the FTIR spectra of both toluene gels are virtually identical (Figure 1 in the Supporting Information), clear differences in the NH and amide I regions are observed in the spectra of the dichloromethane gels (Figure 11, *rac*-**1**: NH 3279 and 3378 cm^{-1}, amide I 1647, 1658, and 1676 cm^{-1}; (*S*,*S*)-**1**: NH 3293 and 3378 cm^{-1}, amide I 1653 and 1676 cm^{-1}). The

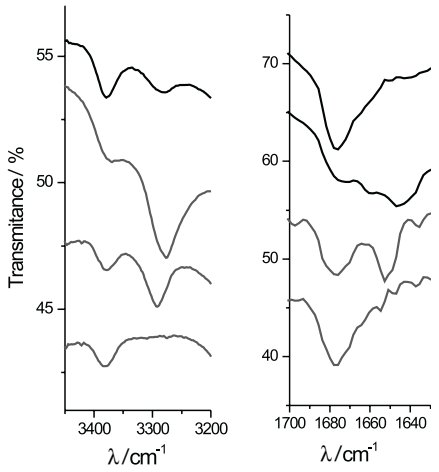

Figure 11. The NH and amide I regions of the FTIR spectra (from top to bottom) for a *rac*-**1** solution, *rac*-**1** gel, (*S*,*S*)-**1** gel, and (*S*,*S*)-**1** solution in dichloromethane.

different positions for the NH and amide I bands correspond to hydrogen-bonded molecules, and result from the diastereomeric relationship between (*S*,*S*)-**1** and the *meso* bilayers of *rac*-**1** (Figure 9).

The formation of waved tapes, which are found in the crystal structure of *rac*-**1**, occurs upon rearrangement of the initially formed *meso* bilayers. The intra-bilayer hydrogen bonding between (*S*,*S*)- and (*R*,*R*)-triads, and the formation of parallel, in-phase shifted tapes is shown schematically in Figure 12. This type of organization contains layers in which the *i*Bu groups are oriented up and down. Moreover, the packing of layers in an orthogonal direction is optimized. It should be noted that formation of such tapes from enatiomeric bilayers (Figure 9c) would require major interbilayer reorganization, and hence, is unlikely. The formation of unstable *rac*-**1** gels that are prone to crystallization in other solvent systems (Table 1) also indicates the presence of *meso* bilayers in those cases.

However, in CCl_4 and a number of aromatic solvents (Table 1), *rac*-**1** forms stable gels that can be kept unchanged for significant periods of time. The following observations can be summarized for the (*S*,*S*)-**1** and *rac*-**1** gels: 1) the X-ray powder diffraction pattern obtained for the crystalline phases separated from the (*S*,*S*)-**1** and *rac*-**1** toluene gels and xerogels are analogous; the pattern closely resembles that obtained for the (*S*,*S*)-**1** single crystal; 2) the FTIR spectra of both toluene gels are very similar; 3) the FTIR spectra of the (*S*,*S*)-**1** and *rac*-**1** dichloromethane gels are different as a result of a diastereomeric relationship between the(*S*,*S*)- and *meso* bilayers present in the gels; 4) *rac*-**1** forms *meso* bilayers in dichloromethane after initial formation of an unstable gel which is prone to crystallization; and 5) *rac*-**1** forms stable gels with toluene, CCl_4, and other aromatic solvents. The observations 1–3 strongly suggest that in toluene gels both (*S*,*S*)-**1** and *rac*-**1** form inverse bilayers. Based on observations 2–5, it would seem that in toluene *rac*-**1** forms bilayers that are not *meso* bilayers. Indeed, the formation of enantiomeric bilayers (Figure 9) best explains the different gelation observed in toluene and other aromatic solvents relative to dichloro-

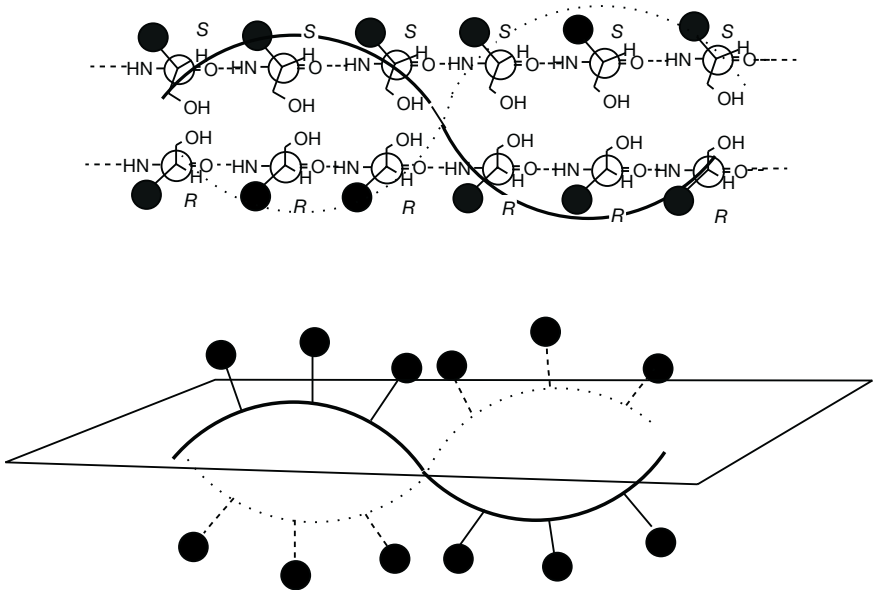

Figure 12. Schematic presentation of the possible intra-*meso* bilayer reorganization of oxalamide–oxalamide hydrogen bonds between (*S*,*S*,*S*,*S*,*S*,*S*)- and (*R*,*R*,*R*,*R*,*R*,*R*)-triads to give the in-plane parallel waved ribbons found in the *rac*-**1** crystal structure.

methane. The following experiment also supports this conclusion. Separate solutions of (*S*,*S*)-**1** and (*R*,*R*)-**1** (3.5 mL) in toluene were prepared, and it was expected that at a concentration of 4.16 mM, which is below the minimal gelation concentration (mgc) of 6.9 mM, aggregated (*S*,*S*)-**1** and (*R*,*R*)-**1** bilayers would be present in the solutions. The two solutions were then mixed at room temperature, but gelation did not occur despite the fact that the *rac*-**1** concentration was higher than its mgc (2.3 mM). However, upon quickly heating and cooling the sample, a stable gel was formed. This experiment shows that the primary (*S*,*S*)–(*S*,*S*) and (*R*,*R*)–(*R*,*R*) bilayer aggregates (Figure 9a) must dissociate and then reaggregate to form the *rac*-**1** gel. In fact, the ^{1}H NMR investigation discussed above indicates that the disaggregation begins within the lipophilic regions at lower temperatures (see preceding paragraph and Figure 2). Therefore, dissociation of the lipophilic regions of (*S*,*S*)–(*S*,*S*) and (*R*,*R*)–(*R*,*R*) aggregated bilayers and their subsequent reaggregation into enantiomerically packed (*S*,*S*)–(*R*,*R*) bilayers (Figure 9c) is expected. As a result, the *rac*-**1** gel fibers possess a higher aspect ratio (see TEM, Figure 1) and have a more compact network, which is able to immobilize larger volumes of toluene. The formation of enantiomeric bilayers (Figure 9c) from (*S*,*S*)–(*S*,*S*) and (*R*,*R*)–(*R*,*R*) bilayers (Figure 9a) should be energetically less demanding, and, hence, faster than a transformation to give *meso* bilayers (Figure 9b). The latter process would require major rearrangement, and include dissociation of the aggregated bilayers in the lipophilic and polar regions, and subsequent reaggregation of the enatiomeric strands.

Conclusion

The bis(amino alcohol) oxalamides **1**–**3** are efficient gelators of various organic solvents and their mixtures. In contrast to bis(amino acid) oxalamides, they lack the ability to form gels with water or highly polar water/DMSO or water/DMF mixtures. Spectroscopic and crystallographic investigations of the toluene gels and the crystals grown from lipophilic solvents reveal that the gelators have a tendency to form reversed bilayers. These are stabilized by cooperative hydrogen bonds, which arise between the oxalamide units and the hydroxymethylene groups. The observed organization can be rationalized upon consideration of the three-dimensional contributions of supramolecular vectors (directional, noncovalent interactions of different energy), as shown in Figure 13.

The potential energy calculations for three dimmers, generated by docking (*S*,*S*)-**1** molecules with oxalamide–oxalamide, OH–OH hydrogen bonds, and lipophilic interactions between *i*Bu groups, respectively, showed that the last two dimers are 40 kJ mol^{-1} less stable than the first.[22] Therefore, the cooperative hydrogen bonds that arise between the oxalamide units (in the *b* plane, two hydrogen bonds per dimer) should have the strongest directional interaction in lipophilic solvents, in which hydrogen bonding is strongly favored. The cooperative hydrogen bonds that occur between OH groups to give one hydrogen bond per dimer (in the *c* plane) involve weaker interactions relative to the oxalamide hydrogen bonds. Finally, the lipophilic interactions (in the *a* plane) are expected to be weakest in lipophilic solvents as a result of efficient solvation. Hence, the fastest organization can be expected to occur in the *b* plane, while self-assembly in the *a* and *c* planes would be much slower. The distribution of aggregation rates based on this hypothesis should lead to the formation of elongated, fibrous aggregates (Figure 11). The rationale presented has some resemblance to the Hartman and Bennema[23] theory of crystal growth; this states that the relative growth rate of a face increases with increasing E_{att}, which is the energy per molecule released when one slice of thickness d_{hkl} crystallizes onto a crystal face (*hkl*). The solvation effects on the apolar (direction *a*) and relatively polar surfaces (directions *b* and *c*) of the initially formed bilayer aggregates should have a strong influence on the energetics of the assembly and, hence, on the fiber aspect ratio. Therefore, these types of gelators fail to gel solvents of high and medium polarity (for example, EtOH, dioxane, THF, EtOAc, acetone), because the solvents can efficiently compete with intermolecular oxalamide–oxalamide hydrogen bonding. In such cases, the formation of smaller aggregates with fiber lengths that are insufficient to form a gel network can be expected. However, the same

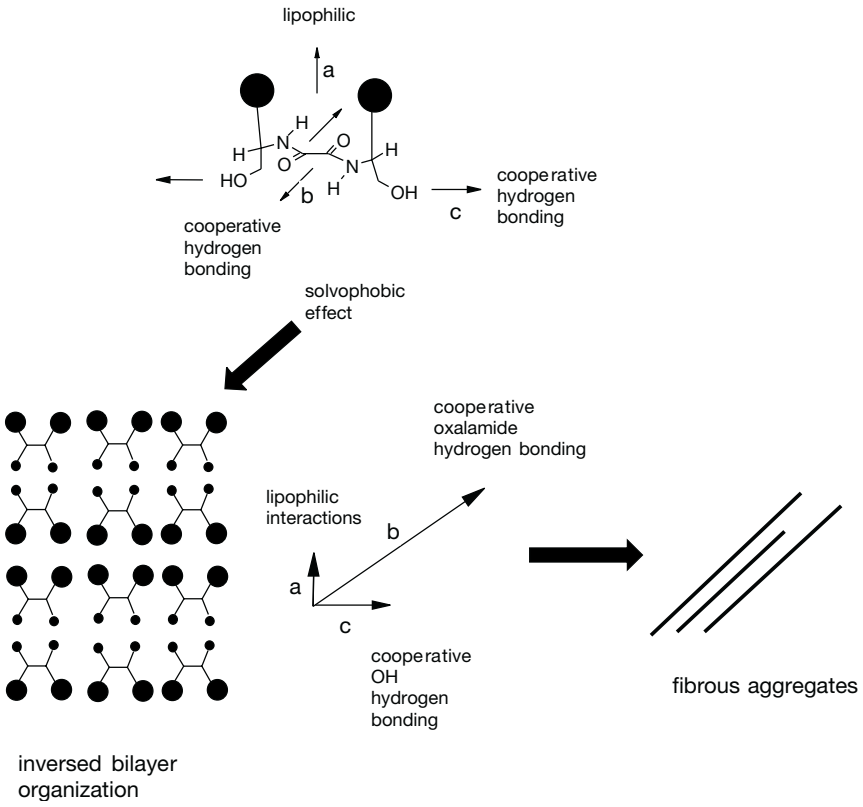

Figure 13. A three-dimensional representation of supramolecular vectors of different strength (**a** lipophilic interactions between bilayers, **b** oxalamide – oxalamide hydrogen bonds, and **c** OH – OH hydrogen bonds). Since $\mathbf{b} \gg \mathbf{a} > \mathbf{c}$, and this determines the aggregation rates, self-assembly into fibrous aggregates should occur. The separation of lipophilic *i*Bu groups (represented by larger filled circles) and polar OH groups (represented by dots) resembles those in amphiphiles, and leads to the formation of inverse bilayers in lipophilic solvents.

compounds are able to gel hexane mixtures of these same solvents (Table 1).

Stereochemistry has a profound influence on gelation properties. In contrast to (*S*,*S*)-**1**, the *meso* diastereoisomer lacks any gelation ability. Although the basic hydrogen-bonding motif for (*S*,*S*)- and *meso*-**1** is similar, the *trans* arrangement of the *i*Bu groups in the latter prevents the formation of a bilayer. The resultant monolayers are subsequently packed centrosymmetrically. This favors crystallization rather than the formation of (*S*,*S*)-**1** chiral bilayers, and explains the gelation ability of the enantiomer and lack of gelation and preferred crystallization of *meso*-**1**. Contrary to previous reports[8], a racemate (*rac*-**1**) was found to gel a volume of toluene three-times larger than the pure enantiomer (*S*,*S*)-**1**. Analysis of the spectroscopic and crystallographic results strongly suggests that *rac*-**1** is able to form *meso* bilayers or enantiomeric bilayers, depending on the properties of the solvent. If *meso* bilayers are formed, crystals of *rac*-**1** or unstable gels, which are prone to crystallization, are obtained. Formation of enantiomeric bilayers affords the stable gels formed by *rac*-**1** with CCl_4 and aromatic solvents (Table 1). The TEM images of (*S*,*S*)-**1** and *rac*-**1** toluene gels showed that the latter consisted of thinner fiber bundles. The result is a more compact network, which is capable of entrapping a larger volume of the solvent. In the series of aromatic solvents tested (Table 1), toluene induced the formation of fibers with the highest aspect ratio.

Experimental Section

General: Melting points were determined on a Kofler stage and are uncorrected. Optical rotations were measured on an optical activity AA-10 automatic polarimetar using the wavelength of 589.3 nm. ^{1}H NMR and ^{13}C NMR spectra were recorded at 300 and 75.5 MHz, respectively, on a Varian XL-300 Gemini spectrometer, and at 500 MHz on a Bruker spectrometer (TMS was used as an internal standard). FTIR spectra were recorded on a Bomen MB 102 spectrometer. Thin-layer chromatography (TLC) was performed on silica-gel-coated Merck 60 F_{254} silica plates, and were visualized using a UV lamp (254 nm) or I_2 vapors. All chemicals were of the best commercially available grade and were used without purification. Solvents were purified according to literature methods and stored over molecular sieves. Compounds **2** and **4** have been described previously.[24]

General procedure for preparation of bis(amino alcohol) oxalyl amides 1 and 3: The respective amino alcohol (4 mmol) was suspended in toluene (10 – 20 mL) and diethyl oxalate (2 mmol) was added as the solution was vigorously stirred. The reaction mixture was stirred and heated at reflux for 1 h. The initially formed solution quickly transformed into a dense gelatinous mass. After cooling to room temperature, the mixture was diluted with isopropyl ether (10 – 20 mL) until the gelatinous mass was destroyed, and the crystalline product was separated by filtration.

***N*,*N*′-Bis[1-(hydroxymethyl)-3-methylbutyl]ethanediamide (1)**: Yield: 88 %; m.p. 175 – 176 °C; $[\alpha]_D^{22} = -26$ ($c = 1$ in DMSO); ^{1}H NMR (300 MHz, [D$_6$]DMSO, 18 °C, TMS): $\delta = 8.2$ (d, ^3J(H,H) = 9.3 Hz, 2H; NH), 4.7 (t, ^3J(H,H) = 5.7 Hz, 2H; OH), 3.9 – 3.8 (m, 2H; CH_α), 3.4 – 3.3 (m, 4H; $CH_{2(\beta')}$–O), 1.5 – 1.4 (m, 4H; $CH_{2(\beta)}$), 1.4 – 1.2 (m, 2H; CH_γ), 0.9, 0.8 ppm (2d, ^3J(H,H) = 6.6 Hz, 12H; $CH_{3(\delta)}$); ^{13}C NMR (75.5 MHz, [D$_6$]DMSO, 20 °C, TMS): $\delta = 159.8$ (CO), 63.4 ($CH_{2(\beta')}$–O), 49.6 (CH_α), 39.5 ($CH_{2(\beta)}$), 21.89 (CH_γ), 23.7, 23.3 ppm ($CH_{3(\delta)}$); IR (KBr): $\tilde{\nu} = 3270$ (NH), 1640 (CONH, amide I), 1500 cm^{-1} (CONH, amide II); elemental analysis calcd (%) for $C_{14}H_{28}N_2O_4$ (288.38): C 58.30, H 9.79, N 9.71; found: C 58.16, H 9.60, N 9.95.

***N*,*N*′-Bis(2-hydroxy-1-phenylethyl)ethanediamide (3)**: Yield: 95 %; m.p. 226 – 227 °C; $[\alpha]_D^{22} = -118$ ($c = 1$ in DMSO); ^{1}H NMR (300 MHz, [D$_6$]DMSO, 20 °C, TMS): $\delta = 9.0$ (d, ^3J(H,H) = 8.5 Hz, 2H; NH), 7.4 – 7.2 (m, 10H; CH_{arom}), 5.1 (br s, 2H; OH), 4.9 – 4.8 (m, 2H; H_α), 3.7 – 3.5 ppm (m, 4H, $CH_{2(\beta')}$–O); ^{13}C NMR (75.5 MHz, [D$_6$]DMSO, 20 °C, TMS): $\delta =$ 157.2 (CO), 137.7 (C_{arom}), 125.6, 124.5 and 124.5 (CH_{arom}), 61.4 ($CH_{2(\beta)}$–O), 53.2 ppm (C_α); IR (KBr): $\tilde{\nu} = 3295$ (NH), 1650 (CONH, amide I), 1510 cm^{-1} (CONH, amide II); elemental analysis calcd (%) for $C_{18}H_{20}N_2O_4 \cdot \frac{1}{2}H_2O$ (337.356): C 64.08, H 6.27, N 8.30; found: C 64.37, H 6.25, N 8.40.

Crystal structure determination of 1, *rac*-1, *meso*-1, and *rac*-2: Intensities were measured on an Enraf Nonius CAD4 diffractometer with graphite monochromated $Cu_{K\alpha}$ radiation of wavelength 1.54178 Å by using the $\omega/2\theta$ scan technique. The crystallographic data and the details for data collection and refinement are listed in Table 9. Significant variations in the intensity of the three control reflections, which were measured every 120 min, were not observed. The data were corrected for Lorentz and polarization effects (data reduction program: XCAD).[25] The absorption correction was based

Table 9. Crystallographic data, structure solution, and refinement of (*S*,*S*)-**1**, *rac*-**1**, *meso*-**1** and *rac*-**2**.

	(*S*,*S*)-**1**	*rac*-**1**	*meso*-**1**	*rac*-**2**
formula	$C_{14}H_{28}N_2O_4$	$C_{14}H_{28}N_2O_4$	$C_{14}H_{28}N_2O_4$	$C_{12}H_{24}N_2O_4$
M_r	288.4	288.4	288.4	260.3
crystal system	monoclinic	monoclinic	triclinic	triclinic
space group	$P2_1$ (No.4)	$C2/c$ (No.15)	$P\bar{1}$ (No.2)	$P\bar{1}$ (No.2)
a [Å]	11.0438(7)	18.092(5)	8.350(6)	5.070(9)
b [Å]	5.0912(3)	17.269(5)	9.986(2)	10.290(5)
c [Å]	15.8761(8)	17.896(5)	11.103(7)	13.770(8)
α [°]			88.89(4)	88.81(3)
β [°]	104.28(5)	107.48(5)	69.21(6)	82.88(3)
γ [°]			84.46(5)	86.29(3)
V [Å^3]	864.9(1)	5333(3)	861(2)	711(1)
Z	2	4	2	2
ρ_{calcd} [g cm^{-1}]	1.110	1.077	1.110	1.216
μ [mm^{-1}]	0.657	0.639	0.657	0.747
T [K]	293(3)	293(3)	293(3)	293(3)
crystal form	prism	prism	prism	prism
crystal size [mm]	$0.2 \times 0.1 \times 0.05$	$0.3 \times 0.1 \times 0.2$	$0.07 \times 0.2 \times 0.3$	$0.005 \times 0.2 \times 0.7$
crystal color	colorless	colorless	colorless	colorless
absorption correction	none	none	ψ-scans	ψ-scans
total data collected	1950	5594	4081	3399
unique data	1796	5428	3576	2850
observed data [$I > 2\sigma(I)$]	1544	3390	2177	1635
R_{int}	0.0279	0.0353	0.056	0.032
θ_{max} [°]	68.8	74.9	75.7	76.8
index range	$-12 \le h \le 13$	$0 \le h \le 22$	$-9 \le h \le 10$	$-6 \le h \le 6$
	$-6 \le k \le 0$	$-20 \le k \le 0$	$-12 \le k \le 12$	$-12 \le k \le 12$
	$-19 \le l \le 0$	$-22 \le l \le 21$	$0 \le l \le 13$	$-17 \le l \le 17$
R_1 [$F_o > 4\sigma(F_o)$]	0.059	0.0871	0.069	0.070
wR_2 (F^2), all data	0.108	0.289	0.232	0.230
S	1.060	1.064	1.140	1.04
parameters	191	280	244	180
largest difference peak/hole [e Å^{-3}]	0.36/−0.22	0.90/−0.35	0.23/−0.18	0.23/−0.29

on a ψ-scan of seven reflections. Structures were solved using the WinGX package,[26] and were refined on F^2 by the SHELXL97 package.[27] Molecular geometry calculations and illustrations of the crystal packing were prepared by PLATON98.[28] Plots of the molecules with thermal ellipsoids scaled at the 30% probability level were prepared by ORTEP.[16] Atomic scattering factors were those included in SHELXL97. The H-atom coordinates were calculated geometrically and refined using the SHELX97 riding model. Compound *rac*-**2** crystallizes as non-merohedral twins in the triclinic space group $P\bar{1}$ (Table 9). The twin axes are [001] reciprocal axes. A detailed treatment of the the twin matrix, evaluation of the intensities of the twin domains, and refinement are beyond the scope of this work and will be published elsewhere. The focus of the crystal structures is the formation of assembled layers through hydrogen bonding, as described above.

CCDC-195966 [(*S*,*S*)-**1**], 195967 [*rac*-**1**], and 195968 [*meso*-**1**] contain the supplementary crystallographic data for this paper. These data can be obtained free of charge via www.ccdc.cam.ac.uk/conts/retrieving.html (or from the Cambridge Crystallographic Data Centre, 12 Union Road, Cambridge CB2 1EZ, UK; (fax: (+44) 1223-336-033; or e-mail: deposit@ccdc.cam.ac.uk)

Acknowledgements

The financial support from the Croatian Ministry of Science and Technology (Projects No. 098053 and 098036) is gratefully acknowledged.

[1] a) P. Terech, R. G. Weiss, *Chem. Rev.* **1997**, *97*, 3133–3159; b) F. S. Schoonbeek, J. H. van Esch, R. Hulst, R. M. Kellog, B. L. Feringa, *Chem. Eur. J.* **2000**, *6*, 2633–2643; c) R. Mukkamala, R. Weiss, *Langmuir* **1996**, *12*, 1474–1482; d) F. M. Menger, K. L. Caran, *J. Am. Chem. Soc.* **2000**, *122*, 11679–11691; e) L. A. Estroff, A. D. Hamilton, *Angew. Chem.* **2000**, *112*, 3589–3592; *Angew. Chem. Int. Ed.* **2000**, *39*, 3447–3450; f) D. J. Abdallah, R. G. Weiss, L*angmuir* **2000**, *16*, 352–355; g) F. Placin, M. Colomes, J.-P. Desvergne, *Tetrahedron Lett.* **1997**, 1665–2668; h) O. Gronwald, S. Shinkai, *Chem. Eur. J.* **2001**, *7*, 4329–4334; i) M. George, R. G. Weiss, *J. Am. Chem. Soc.* **2001**, *123*, 10393–10394.

[2] R. J. P. Corriu, D. Leclercq, *Angew. Chem.* **1996**, *108*, 1524–1540; *Angew. Chem. Int. Ed. Engl.* **1996**, 35, 1420–1436.

[3] a) J. van Esch, F. Schoonbeek, M. de Loos, E. M. Veen, R. M. Kellog, B. L. Feringa, *Nato ASI Ser. Ser. C* **1999**, *527*, 233–259; b) K. Murata, M. Aoki, T. Suzuki, T. Harada, H. Kawabata, T. Komori, F. Ohseto, K. Ueda, S. Shinkai, *J. Am Chem. Soc.* **1994**, *116*, 6664–6676; c) J. L. Pozzo, G. Clavier, F. Rustmeyer, H. Bouas-Laurent, *Mol. Cryst. Liq. Cryst.* **2000**, *344*, 101–106; d) J. L. Pozzo, G. Clavier, J. P. Desvergne, *J. Mater. Chem.* **1998**, *8*, 2575–2577.

[4] a) S. Bhattacharaya, Y. Krishnan-Ghosh, *Chem.Commun.* **2001**, 185–186; b) K. Hanabusa, A. Itoh, M. Kimura, H. Shirai, *Chem. Lett.* **1999**, 767–768.

[5] a) M. de Loos, J. van Esch, R. M. Kellog, B. L. Feringa, *Angew. Chem.* **2001**, *113*, 633–636; *Angew. Chem. Int. Ed.* **2001**, *40*, 613–616; b) G. Meiden-Gundert, L. Klein, M. Fischer, F. Vögtle, K. Heuze, J.-L. Pozzo, M. Vallier, F. Fages, *Angew. Chem.* **2001**, *113*, 3266–3267; *Angew. Chem. Int. Ed.* **2001**, *40*, 3164–3166; c) J. van Esch, S. De Feyter, R. M. Kellog, F. De Schryver, B. L. Feringa, *Chem. Eur. J.* **1997**, *3*, 1238–1243; d) K. Hanabusa, Y. Matsumoto, T. Miki, T. Koyama, H. Shirai, *J. Chem. Soc. Chem. Commun.* **1994**, 1401–1402; e) K. Hanabusa, M. Yamada, M. Kimura, H. Shirai, *Angew. Chem.* **1996**, *108*, 2086–2088; *Angew. Chem. Int. Ed. Engl.* **1996**, *35*, 1949–1951.

[6] a) H. Kobayashi, A. Friggeri, K. Koumoto, M. Amaike, S. Shinkai, D. Reinhoudt, *Org. Lett.* **2002**, *4*, 1423–1426; b) O. Gronwald, S. Shinkai, *J. Chem. Soc. Perkin Trans. 2* **2001**, 1933–1937; c) T. Ishi, Y. Ono, S. Shinkai, *Chem. Lett.* **2000**, 808–809; d) K. Yoza, N. Amanokura, Y. Ono, T. Akao, H. Shinomori, M. Takeuchi, S. Shinkai, D. Reinhoudt,

Chem. Eur. J. **1999**, *5*, 2722 – 2729; e) O. Gronwald, K. Sakurai, R. Luboradzki, T. Kimura, S. Shinkai, *Carbohydr. Res.* **2001**, *331*, 307 – 318.
[7] a) M. Jokić, J. Makarević, M. Žinić, *J. Chem. Soc. Chem. Commun.* **1995**, 1723 – 1724; b) R. Oda, I. Huc, *Angew. Chem.* **1998**, 110, 2853 – 2858; *Angew. Chem. Int. Ed.* **1998**, *37*, 2689 – 2691.
[8] a) X. Luo, B. Liu, Y. Liang, *Chem. Commun.* **2001**, 1556 – 1557; b) K. Hanabusa, H. Kobayashi, M. Suzuki, M. Kimura, H. Shirai, *Colloid Polym. Sci.* **1998**, *276*, 252 – 259; c) K. Hanabusa, K. Okui, K. Karaki, M. Kimura, H. Shirai, *J. Colloid Interface Sci.* **1997**, *195*, 86 – 93; d) S. Bhattacharya, S. N. Ghanashyam Acharya, A. R. Raju, *Chem. Commun.* **1996**, 2101 – 2102.
[9] J.-H. Fuhrhop, P. Schneider, J. Rosenberg, E. Boekema, *J. Am. Chem. Soc.* **1987**, 109, 3387 – 3390.
[10] P. Terech, V. Rodriguez, J. D. Barnes, G. B. McKenna, *Langmuir* **1994**, *10*, 3406 – 3418.
[11] J. Makarević, M. Jokić, B. Perić, V. Tomišić, B. Kojić-Prodić, M. Žinić, *Chem. Eur. J.* **2001**, *7*, 3328 – 3341.
[12] S. Luboradzgi, R. Gronwald, O. Ikeda, A. Shinkai, *Chem. Lett.* **2000**, 1148 – 1149.
[13] a) F. Menger, Y. Yamasaki, K. K. Catlin, T. Nishimi, *Angew. Chem.* **1995**, *107*, 616 – 618; *Angew. Chem. Int. Ed. Engl.* **1995**, *34*, 585 – 586; b) D. C. Duncan, D. G. Whitten, *Langmuir* **2000**, *16*, 6445 – 6452.
[14] IUPAC – IUBMB Biochemical Nomenclature: *Pure Appl. Chem.* **1997**, *69*, 2475 – 2487.
[15] C. K. Johnson, M. N. Burnett, ORTEP-III, Report ORNL-6895, Oak Ridge National Laboratory, Tennessee (USA), **2000**.
[16] J. Bernstein, R. E. Davies, L. Shimoni, N.-L. Chang, *Angew. Chem.* **1995**, *107*, 1689 – 1708; *Angew. Chem. Int. Ed. Engl.* **1995**, *34*, 1555 – 1573.
[17] S. Coe, J. J. Kane, T. L. Nguyen, L. M. Toledo, E. Winiger, F. W. Fowler, J. W. Lauher, *J. Am. Chem. Soc.* **1997**, *119*, 86 – 93.
[18] I. L. Karle, D. Ranganathan, K. Shah, N. K. Vaish, *Int. J. Pept. Protein Res.* **1994**, *43*, 160 – 165.
[19] I. L. Karle, D. Ranganathan, *Int. J. Pept. Protein Res.* **1995**, *46*, 18 – 23.
[20] I. L. Karle, D. Ranganathan, *Int. J. Pept. Protein Res.* **1995**, *46*, 24 – 29.
[21] I. L. Karle, D. Ranganathan, *Biopolymers* **1995**, *36*, 323 – 331.
[22] SYBYL Version 6.3 software from TRIPOS Inc. The starting molecule was taken from the crystal structure of (*S*,*S*)-**1**. The systematic conformational search using the TRIPOS force field was done in 30° increment rotations for all rotable bonds. The lowest-energy conformation, which was generated by full minimization, differs very slightly from the X-ray molecular structure. Dimers were generated by using the Docking module of the software and were fully minimized.
[23] P. Hartman, P. Bennema, *J. Cryst. Growth* **1980**, *49*, 145 – 156.
[24] S. E. Denmark, R. A. Stavenger, A. M. Faucher, J. P. Edwards, *J. Org. Chem.* **1997**, *62*, 3375 – 3389.
[25] K. Harms, S. Wocadlo, XCAD4-CAD4 Data Reduction, University of Marburg, Marburg (Germany), **1995**.
[26] WinGX: L. J. Farrugia, *J. Appl. Crystallogr.* **1999**, 32, 837 – 838.
[27] G. M. Sheldrick, SHELX97, Program for the Refinement of Crystal Structures, University of Göttingen, Göttingen (Germany), **1997**.
[28] A. L. Spek, PLATON98, A Multipurpose Crystallographic Tool 101201 Version, University of Utrecht, Utrecht (The Netherlands), **2001**.

Received: November 12, 2002
Revised: June 27, 2003 [F4573]